Adjusting for Long-Term Anomalous Trends in NOAA's Global Vegetation Index Data Sets

Le Jiang, J. Dan Tarpley, Kenneth E. Mitchell, Sisong Zhou, Felix N. Kogan, and Wei Guo

***Abstract*—The weekly 0.144° resolution global vegetation index from the National Oceanic and Atmospheric Administration (NOAA) National Environmental Satellite, Data, and Information Service (NESDIS) has a long history, starting late 1981, and has included data derived from Advanced Very High Resolution Radiometer (AVHRR) sensors onboard NOAA-7, -9, -11, -14, -16, -17, and -18 satellites. Even after postlaunch calibration and mathematical smoothing and filtering of the normalized difference vegetation index (NDVI) derived from AVHRR visible and near-infrared channels, the time series of global smoothed NDVI (SMN) still has apparent discontinuities and biases due to sensor degradation, orbital drift [equator crossing time (ECT)], and differences from instrument to instrument in band response functions. To meet the needs of the operational weather and climate modeling and monitoring community for a stable long-term global NDVI data set, we investigated adjustments to substantially reduce the bias of the weekly global SMN series by simple and efficient algorithms that require a minimum number of assumptions about the statistical properties of the interannual global vegetation changes. Of the algorithms tested, we found the adjusted cumulative distribution function (ACDF) method to be a well-balanced approach that effectively eliminated most of the long-term global-scale interannual trend of AVHRR NDVI. Improvements to the global and regional NDVI data stability have been demonstrated by the results of ACDF-adjusted data set evaluated at a global scale, on major land classes, with relevance to satellite ECT, at major continental regions, and at regional drought detection applications.**

***Index Terms*—Advanced Very High Resolution Radiometer (AVHRR), land surface, normalized difference vegetation index (NDVI), remote sensing, satellite-based vegetation, vegetation index.**

I. Introduction

THE WEEKLY global vegetation index (GVI) at 0.144° resolution developed and maintained by the National Oceanic and Atmospheric Administration (NOAA) National Environmental Satellite, Data, and Information Service (NESDIS) [1], [2] has been produced since late 1981. This GVI data set includes different generations of Advanced Very High Resolution Radiometer (AVHRR) sensors onboard NOAA polar-orbiting satellites. For the Second Generation GVI (denoted GVI2 hereafter), operational weekly composite values of AVHRR channels, along with satellite scan angles and solar zenith angles, corresponding to weekly (i.e., seven days) maximum value composites (MVCs) of normalized difference vegetation index (NDVI) are saved into arrays having dimensions of 2500 pixels (west to east) by 904 pixels (north to south), covering the region of 55°S to 75°N. NESDIS used all of the afternoon overpass satellites (e.g., NOAA-7, -9, -11, -14, -16, and -18), as well as some of the morning overpass satellite data (e.g., NOAA-17) when the afternoon overpass satellite malfunctioned, to composite the long-term GVI2 data set.

Although the NOAA GVI2 data sets and derived products are used to monitor global and regional vegetation conditions and to investigate droughts and other climate impacts on the land surface, the current GVI2 data set has no climate data record (CDR) quality due to numerous errors associated with sensor degradation, orbit drift (which impacts the viewing geometry, e.g., sun angle of the acquisition, resulted in changes in the measurements), and variation of sensor response functions among different AVHRR sensors.

When operationally producing the NOAA weekly GVI2, the MVC scheme reduces cloud contamination at the weekly interval. However, impact of persistent cloud cover (longer than the compositing period) cannot be fully removed. In the past, to use the GVI2 data set for regional drought monitoring, additional multistep mathematical smoothing and filtering were applied to the weekly NDVI to reduce impact of persistent cloudiness [3]. Drought monitoring indexes based on smoothed NDVI (denoted SMN) have shown great success in detecting regional droughts worldwide [3]–[6].

NDVI is calculated as $\mathrm{NDVI} = (\rho_{\mathrm{NIR}} - \rho_{\mathrm{VIS}})/(\rho_{\mathrm{NIR}} + \rho_{\mathrm{VIS}})$, where ρ_{VIS} is the remotely sensed surface reflectance in visible (VIS) band in the red portion of the spectrum where chlorophyll absorption is maximal, and ρ_{NIR} is the reflectance in near-infrared (NIR) band where light reflectance from the plant canopy is dominant. For AVHRR, these are channel 1 (visible band: 0.58–0.68 μm) and channel 2 (near-infrared band: 0.72–1.1 μm). NDVI measured greenness and vigor of vegetation [7] and correlated with the fraction of photosynthetically active radiation absorbed by vegetation [8]. In this paper, we use NDVI as a proxy for surface vegetation greenness for simplicity. SMN, however, does not remove biases or long-term trend in the global NDVI time series. Fig. 1 shows the

Manuscript received February 15, 2007; revised May 14, 2007. This work was supported in part by I. M. Systems Group, Inc. (IMSG), the National Oceanic and Atmospheric Administration (NOAA) National Environmental Satellite, Data, and Information Service (NESDIS) Center for Satellite Applications and Research (STAR) fund under Contract GS-10F-0158N/DG133E-05-NC-2158, and in part by an IMSG corporate science development fund.

L. Jiang and W. Guo are with IMSG, NOAA/NESDIS, Camp Springs, MD 20746 USA.

J. D. Tarpley and F. N. Kogan are with STAR, NOAA/NESDIS, Camp Springs, MD 20746 USA (e-mail: Dan.Tarpley@noaa.gov).

K. E. Mitchell is with the Environmental Modeling Center, NOAA National Centers for Environmental Prediction, Camp Springs, MD 20746 USA.

S. Zhou, retired, was with IMSG, NOAA/NESDIS, Camp Springs, MD 20746 USA.

Color versions of one or more of the figures in this paper are available online at http://ieeexplore.ieee.org.

Digital Object Identifier 10.1109/TGRS.2007.902844

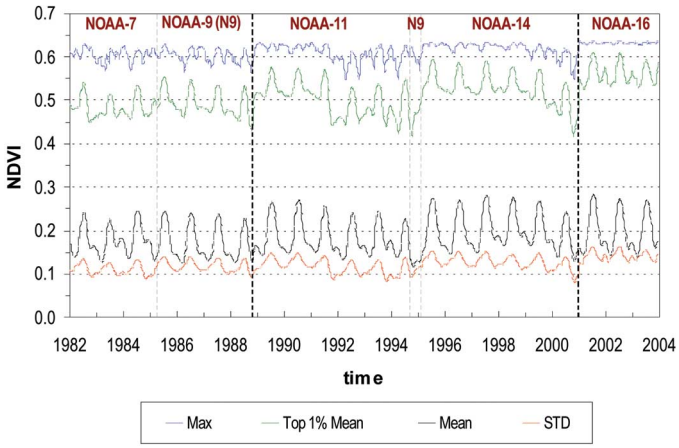

Fig. 1. Weekly global SMN time series of maximum, mean of top 1% highest, mean, and standard deviation of global NDVI.

time series curves for the 1) maximum; 2) mean of top 1%; 3) mean; and 4) standard deviation of the weekly global SMN for 22 years from 1982 to 2003. Among these 22 years, a number of years' data have very poor quality for obvious reasons. For example, the NDVI decrease from 1988 to 1989 is due to the serious degradation of NOAA-9; the NDVI decrease from 1991 to 1992 is likely due to volcanic ash from the Mt. Pinatubo eruption in June 1991 [9]; and the NDVI decrease from late 1994 to early 1995 is due to replacement of NOAA-11 by NOAA-9 (which was already seriously degraded). These events are evident from the mean value and the mean of top 1% curves in Fig. 1. These SMN fluctuations are "noise," in the sense that they are not related to true vegetation anomalies. Given the operational constraints and difficulties using ground truth observations to correct different AVHRR channels, full physically based corrections that could compensate for 1) *satellite orbit drifting and sensor degradation;* 2) *differences in AVHRR sensor response functions;* and 3) *contamination from atmospheric water vapor and aerosols* were not feasible when producing the GVI2 data sets. Consequently, despite the aforementioned mathematical smoothing and filtering, long-term biases and trends in global SMN data sets are still present. Fig. 1 also indicates that there are other trends that do not arise for obvious reasons, such as the drop of peak values (in the mean value and the mean of top 1% value curves) in 1983 and the rise of standard deviation values after 2001. The most important use of the AVHRR NDVI at NOAA is to initialize the surface physics modules running in the operational numerical weather prediction (NWP) models. To do this, the current (for the latest week) green vegetation fraction (GVF) will be derived from the operational GVI2 products and will be delivered to the NWP models in future operations. The GVF is used by the NWP models to partition the surface energy fluxes between direct evaporation from bare soil and evaporation from the vegetation canopy and transpiration through the canopy. NDVI can be directly rescaled into surface GVF [10], which parameterizes land surface evaporation and transpiration in the models. Accurate knowledge of surface GVF helps improve multiple components of surface evapotranspiration terms [11] that improve near-surface temperature and humidity forecasts. For this use, the GVF must reflect vegetation anomalies caused by droughts and periods of higher-than-normal rainfall. To accurately achieve this, the GVF (and the underlying NDVI) must be free of noise and trends caused by atmospheric effects and instrument-to-instrument variability. The work described below is an attempt to reduce the noise and trends in the data without removing information about vegetation anomalies caused by short-term (weeks to months) weather fluctuations.

Ideally, an algorithm to fix the discrepancies in the NDVI time series should meet the following goals: 1) *remove the inconsistencies caused by false signals (or noise) as well as the nonphysical systematic errors* and 2) *retain and enhance the true signal so that seasonal and annual vegetation anomalies can be quantified*. More importantly, the algorithm should have components to correct biases related to each error source with full physics-based adjustments. However, in reality, full physics-based adjustment often requires additional observation data/parameters, which makes correction impossible in real time or unsound when the solution involves more unknowns than measurable quantities. Such dependency (on other observed or model derived parameters) may result in larger errors in operational production and undesirable computational and production complexity. Data independency is one of our key requirements for developing operational systems that can efficiently generate products.

In this paper, rather than investigating complicated physics-based methods that need additional data or computationally expensive empirical time series decomposition/reconstruction approaches, we will use a number of mathematical and statistical approaches with the goal of making it usable in real time within the operational environment constraints at NOAA/NESDIS.

The adjustment approaches are all based on straightforward assumptions of global statistical stationarity of the land surface vegetation. Such stationarity assumptions eliminate the possibility of using the adjusted data sets to assess global-scale net interannual NDVI changes over the past two decades; nevertheless, such assumptions do *not* preclude using the adjusted NDVI to reveal regional or local vegetation anomalies.

The key purpose of this paper is to deliver an operationally feasible algorithm that can produce a more internally consistent and improved quality NDVI data set for the NOAA/NESDIS operational vegetation processing data stream. In particular, we have:

- investigated a number of mathematical and statistical adjustment methods;
- evaluated the global statistical properties and implications of SMN data sets adjusted by different methods;
- evaluated the performance of the adjusted SMN data sets on global major land type classes, major continental regions, and on the relevance to polar-orbiting satellite equator crossing time (ECT);
- demonstrated the usefulness of the adjusted NDVI for regional drought detection.

The corrections/adjustments that we have investigated in this paper can be easily implemented in operations without interfacing with other data sources that would prohibit a real time implementation. We must emphasize that the data sets

processed will not address issues related to global warming and global-scale surface vegetation trend over the past two decades. Nevertheless, regional-scale vegetation anomaly studies are not affected. Further discussion on this issue will be provided in Section IV. The adjusted global NDVI data sets should be interpreted as the top of atmosphere (TOA) quantities.

Section II describes the characteristics of the AVHRR data (in Section II-A), the necessity of a benchmark weekly NDVI climatology (in Section II-B), and a variety of single-step approaches as well as combinational approaches (in Section II-C). The results of different approaches are evaluated and compared to each other in Section III, which also includes the evaluation with respect to regional droughts. Section IV provides a further discussion on the pros and cons of the adjustment approaches investigated in this paper. Section V concludes this paper.

II. Approaches to Adjust the Long-Term Anomalous Trends in Global NDVI Data Sets

A. Data Description

GVI2 data sets are composed of data from NOAA-7 (week 35 of 1981 to week 14 of 1985), NOAA-9 (week 15 of 1985 to week 44 of 1988, as well as week 37 of 1994 to week 6 of 1995 when NOAA-11 data were not reliable), NOAA-11 (week 45 of 1988 to week 36 of 1994), NOAA-14 (week 7 of 1995 to week 52 of 2000), NOAA-16 (week 1 of 2001 to week 11 of 2004), NOAA-17 (week 12 of 2004 to week 34 of 2005), and NOAA-18 (week 35 of 2005 to present). In this paper, our sample data sets will include SMN from week 1 of 1982 to week 52 of 2003, a total of 22 annual cycles.

The best available calibration was applied to the weekly composite AVHRR visible (VIS) and near-infrared (NIR) channels (based on NDVI MVC) using the methods described by Rao and Chen [12] for NOAA-7 to NOAA-14 and by Wu [13] for NOAA-16. After NDVI is calculated from these channels, a temporal smoothing filter was applied to obtain the SMN series. The smoothing technique was designed as a 15-week moving filter that includes multiple steps (such as gap filling, five-week median filtering, and 15-week smoothing using a predefined varying coefficient weighting function). The filter helped to tremendously reduce the high-frequency fluctuations such as those due to cloud and short-term weather changes [3], [14]. The resulting SMN data sets are the subject of our study. On the other hand, due to the use of the 15-week smoothing filter, the near real-time operational process will have the unstable end-of-time-series issue commonly seen in most of the smooth filtering techniques. Similar to many other operational weather products, this is overcome by distinguishing the real time products into "initial early product" (which is the earliest possible product in real time at the end of the smoothing filter), "final update product" (which is the best quality product taking full advantage of the smoothing filter and not further affected by updated real time data, lying in the middle of the smoothing filter), and "temporary product" (which lies between the final update product and the initial early product and gets updated each week when new data are processed by the smoothing filter). Given our design of the 15-week smoothing filter, "final update product" is seven weeks behind real time, whereas "initial early product" is generated for just the past week. In this paper, if no explicit explanation is provided, we use "NDVI" to mean "SMN."

As shown in Fig. 1, the time series of 1) global maximum NDVI (which compose of the maximum single-pixel NDVI value from each week's global NDVI map); 2) mean of top 1% NDVI value; and 3) global NDVI standard deviation are plotted. The curve of global minimum NDVI value is not shown since it is very close to zero and uniform over time. Obviously, the weekly global mean NDVI of the earlier satellites of NOAA-7 and NOAA-9 are lower than those of NOAA-11, -14, and -16. The abnormally low mean annual value of NDVI in 1988 was due to the serious degradation of NOAA-9 as well as the very late local time of observation (e.g., 4–5 P.M.). The abnormally low annual values of NDVI near the end of 1994 to the beginning of 1995 was due to the substitution of NOAA-9 for NOAA-11 (which was already in serious degradation) just to operationally continue the time series.

B. Benchmark NDVI Climatology From Years With High Data Quality

Overall, the global maximum NDVI in each weekly map represents the Earth's "greenest" vegetation in a proxy sense, regardless of the seasonal cycles in different latitude or climate zones. Such value, although its exact pixel location will vary, should be relatively invariant given that fully vegetated areas always exist at any given week on Earth. For example, the tropical forests are always covered with nearly full vegetation, given the abundant rainfall and favorable temperature for vegetation growth in tropical zones, whereas seasonal cycles for other regions of the Earth will have dominant effects. The Northern and Southern Hemispheres have reversed seasonal cycles, so when one is in winter or pregrowing season, the other will be in summer or postgrowing season. For a given tropical forest region, the highest NDVI values may not always be detectable from satellite due to frequent and persistent cloud cover. However, it is unlikely that the whole tropical forested regions of the Earth will be all covered by cloud at any given week. Further, in many nontropical regions, when the full vegetated season is reached, the maximum NDVI (detected from space) in these regions can be as large as or larger than those on the tropical forest. These factors cause the global maximum value of the observed NDVI from satellite to be very stable from week to week and from year to year, given the very large total number of pixels over the Earth's land surface. Close examination of the weekly maximum NDVI (i.e., $\mathrm{ND}_{\max}$) time series in Fig. 1 shows that this parameter is not always stable as it should be if our reasoning of the "stable global maximum" NDVI above is sound. After we further examined the maximum NDVI time series, as we expanded the plot of the same data series in Fig. 1 into 22 annual cycles, we found that weekly maximum NDVI is relatively more stable in years 1989, 1990, 1995 (after week 14), and 1996–1998. These were the stable performance periods of NOAA-11 and NOAA-14, during which the weekly global NDVI data have relatively high quality. For all these years, the NOAA polar-orbiting satellites have local observation time

TABLE I
LIST OF GLOBAL NDVI ADJUSTMENT APPROACHES EVALUATED

Approach to be evaluated	Methodology	Description
a. and b. Range Re-Scaling (RRS)	$\frac{ND - ND_{\min}}{ND_{\max} - ND_{\min}} = \frac{ND_0 - ND_{0\min}}{ND_{0\max} - ND_{0\min}}$ (1), where for a given week, ND is the known NDVI for a pixel, $ND_{\max}$ and $ND_{\min}$ are the maximum and minimum NDVI respectively within a global map. $ND_{0\max}$ and $ND_{0\min}$ are the maximum and minimum NDVI of the benchmark global NDVI map for that week. ND_0 is therefore the "equivalent" NDVI for ND within the context of the benchmark map.	Solve ND_0 within the context of benchmark climotology a). Use pixel maximum ND as ND_{max}; b). Use the average of the top 1% maximum ND as ND_{max}
c. Normalization (NML)	$\frac{ND - \overline{ND}}{\sigma_{ND}} = \frac{ND_0 - \overline{ND_0}}{\sigma_{ND_0}}$ (2), where ND and ND_0 have the same general meanings as those in Equation (1), $\overline{ND}$ and σ_{ND} are the global mean and standard deviation of NDVI for a certain week in real-time. $\overline{ND_0}$ and σ_{ND_0} are the global mean and standard deviation of the benchmark climatology for that week.	Solve ND_0 within the context of benchmark climotology
d. Linear Regression (LR)	$ND_0 = a + b \cdot ND$ (3), where ND and ND_0 interpreted similarly as before, a and b are the linear regression coefficients from the scatter plot of global NDVI vs. benchmark global NDVI for a certain week	
e. Adjusted Cumulative Distribution Function (ACDF)	Adjust the problematic weekly global NDVI such that for a certain week, the adjusted cumulative distribution function (CDF) or empirical distribution function (EDF) matches the CDF of the benchmark (i.e., 6-yr climatology).	See Figure 2.
f. NML+RRS	NML followed by RRS	
g. Adjusting Satellite-By-Satellite (ASBS)+NML	Make adjustment satellite-by-satellite, then further line up values among different satellites by adjusting the differences among satellites.	

between 1:30 P.M. and 3:00 P.M. We selected the above six years as reference to form the benchmark weekly climatology of NDVI. (Additionally, years 2001, 2002, and 2003 of NOAA-16 data appear also to be good, except for the systematic yet stable overestimate of NDVI compared to other years—most likely caused by the narrower AVHRR sensor spectral bands in the VIS and NIR channels.) Weekly global SMN from these six years are averaged and used as a benchmark for adjusting other years' data using approaches described in Section II-C.

C. Approaches

We will evaluate a number of single-step and combinational approaches. These are highlighted below. Further detailed descriptions of these approaches are provided in Table I.

1) Range rescaling (RRS)—The basic idea of RRS is to use the weekly global NDVI from a reliable year or best known short multiyear period (with little trend in the given NOAA satellite platform) as benchmark data set, then rescale weekly NDVI in other years within the proper maximum and minimum NDVI range prescribed by the benchmark data set. Referring to (1) in Table I, although the minimum NDVI ($\mathrm{ND}_{\min}$) is very close to zero (i.e., $\mathrm{ND}_{\min} \approx 0.0$), we have the option to select $\mathrm{ND}_{0\max}$ and $\mathrm{ND}_{\max}$ as the absolute maximum NDVI within the weekly global NDVI map, or as the mean of, for example, top 1% highest NDVI value pixels. The latter may overcome the statistical limitation of picking the maximum NDVI value from a single pixel of the weekly global NDVI map. See Table I for options a and b.
2) Normalization (NML)—Statistically normalized quantities from two different sample spaces are often found to be equivalent to one another when one sample space is a linear transform of another or vise versa. Assuming statistically normalized global NDVI is stationary for the same week of different years, we can use the benchmark climatology as standard and adjust other years' weekly NDVI within the standardized or normalized range. See option c in Table I.
3) Linear regression (LR)—This is another straightforward approach that can transform linearly biased samples to standard level with the latter given by the benchmark climatology. See option d in Table I.

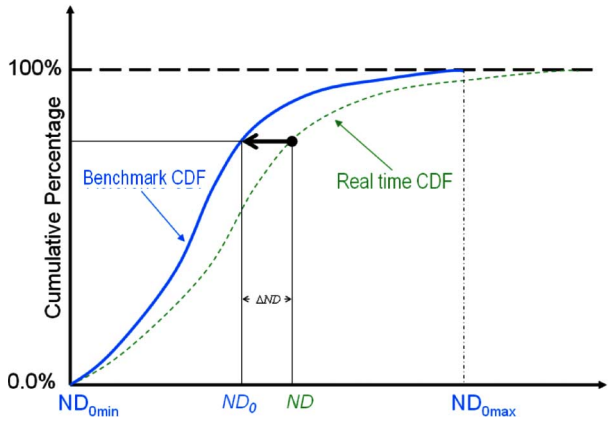

Fig. 2. Schematic illustration of the CDF adjustment approach. In the adjustment process, real time global NDVI is adjusted such that the ACDF matches the benchmark CDF.

4) Adjusted cumulative distribution function (ACDF)—This approach is to adjust the weekly global NDVI such that for a certain week, the ACDF matches the CDF of the benchmark (i.e., six-year climatology). A schematic illustration of this approach is provided in Fig. 2. This is a nonlinear approach since different NDVI values will be differently adjusted depending on how the corresponding cumulative probability in the to-be-adjusted data set is different from that of the benchmark. After the adjustment, the CDFs are identical for the weekly global NDVI and the benchmark. The underlying assumption is that global vegetation for a certain week is stationary in terms of total amount and the net amount within each NDVI interval. Only the spatial distribution of global NDVI may be different. Considering that the historical global precipitation is not stationary even at monthly time scales, the assumption in this approach may be too strict in that it eliminates global interannual variations for the same week of different years. However, the assumption has no mechanism to constrain spatial distribution of weekly global NDVI, which is a desirable feature that allows the adjusted NDVI to be used to reasonably detect local or regional NDVI changes, droughts, or vegetation stress. Further, the original highs and lows of NDVI within the weekly global map will not change in a relative sense, although the absolute magnitudes are adjusted. The results from the ACDF approach are summarized in Section III. For other descriptions for this method, see option e in Table I.
5) NML followed by RRS—Our criteria to evaluate the effects of different approaches are simple: whether anomalous/spurious trends in weekly global NDVI time series are removed and whether the range of NDVI values within a global map is reasonable (e.g., consistent from week to week). The first can be examined by determining if the trend in the global mean NDVI time series has been removed after adjustment. The second is met if we have got rid of the variations in the range of NDVI (marked by $\mathrm{ND}_{\max}$ and $\mathrm{ND}_{\min}$, or by the top 1% maximum ND and $\mathrm{ND}_{\min}$). Since $\mathrm{ND}_{\min}$ is always close to zero, the effects can be seen in the $\mathrm{ND}_{\max}$ time series. As will be described in Section III, most of the single-step approaches cannot simultaneously meet both criteria. The difference is in the relative extent to which these approaches can meet the above criteria. A combinational approach, which, for example, uses the RRS or NML as a second step, may help fix the global NDVI ranges after major discrepancies are eliminated in global NDVI mean time series.
6) Adjusting satellite-by-satellite (SBS) followed by NML—One shortcoming of the above simple adjustment approaches is in the need to use a benchmark of a whole annual cycle of weekly global NDVI, which comes from the believed-to-be best climatology from a subset of the 22-year data record. It is expected that the global NDVI after adjustment will be similar to the six-year climatology (in terms of global statistical metrics), which makes it hard for the adjusted data set to detect any global-scale NDVI trend over the period of record. Issues with this limitation will be further described in Section IV.

To eliminate the need for a benchmark weekly NDVI climatology, an alternative is to make adjustment SBS, then further line up values among different satellites by adjusting the differences. For example, considering that each satellite underwent initial in-flight stable operation, then drift to a much later ECT and sensor degradation in a gradual fashion, we can assume data from the first year of each satellite's stable operation have relatively high quality, then adjust the follow-on years' NDVI values to the same level to that of the first year. Using a similar equation, as (2) in Table I, but with $\overline{\mathrm{ND}_0}$ and σ_{ND_0} representing the mean and standard deviation of a certain weekly global NDVI for the first year, respectively, and $\overline{\mathrm{ND}}$ and σ_{ND} representing the corresponding metrics for the to-be-adjusted week in another year, respectively, then the equivalent NDVI (to the level of the first year) after adjustment can be easily calculated by this equation. As such, we selected years 1982 for NOAA-7, 1986 for NOAA-9, 1989 for NOAA-11, 1996 for NOAA-14, and 2001 for NOAA-16, and made the adjustment SBS.

After such adjustment, different years' global NDVI data for a same satellite should be at the same level. In other words, global bias due to the same sensor degradation and orbit drifting is gone. However, as expected, there will still be discrepancies among different satellites after this step due to differences in the designed VIS and NIR band sensor response functions as well as the atmospheric contamination effects associated with these response functions. A combinational approach, for example, using the NML as a second step, may help to remove the major discrepancies caused by different satellites.

Approaches 1), 2), and 3) are essentially linear under the assumption that the global mean NDVI time series is stationary, and the two sample spaces (i.e., real-time weekly global NDVI space and benchmark weekly global NDVI space) are linearly related. Approach 4) is nonlinear, whereas approaches 5) and 6) are composed of linear steps. Further, all of these approaches assume the global stationary property of the weekly NDVI but do not constrain the local vegetation spatial variation.

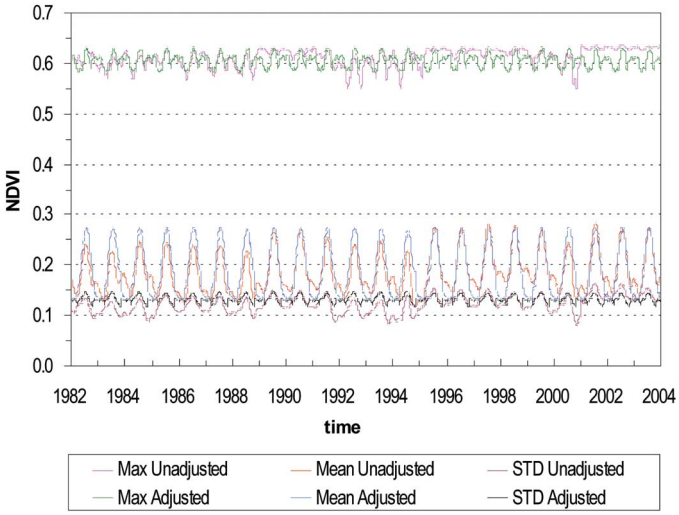

Fig. 3. Maximum, mean, and standard deviation of global NDVI before and after ACDF adjustment.

III. Results

A. Results of Different Single and Combinational Approaches

For brevity, results for different adjustments described in Section II are summarized, without presenting numerous figures to demonstrate the details for each case, as follows.

- The RRS approach makes the range of NDVI consistent from year to year as expected. It appears not to fix the bias in global mean, either by selecting ND_{max} as the absolute maximum NDVI or as the average of the top 1% highest NDVI within the weekly global NDVI map.
- The NML approach fixes the problem in global mean; however, it causes problems and more variations in the range (indicated by the maximum NDVI series after adjustment).
- The LR approach fixes the trend in the global mean NDVI; however, similar to the NML approach, it is unable to fix the problem in the maximum global NDVI series.
- The ACDF approach is able to fix the trend in the global mean NDVI, while global maximum NDVI series shows great improvement (i.e., much smaller variation than the unadjusted NDVI).
- NML followed by RRS (NML_RRS) fixed the problems in maximum NDVI time series; however, it left problems in the global mean NDVI time series.
- Adjusting SBS followed by mean value adjustment among different satellites using NML (SBS_NML) approach appears to result in a similar product as the NML or LR approach.

Of the approaches tested, the ACDF method was the best in terms of both making the mean NDVI time series align better among years and reducing the range of variation for the maximum NDVI series. Fig. 3 shows the adjusted maximum, mean, and standard deviation curves compared to the unadjusted ones. The adjusted maximum NDVI exhibit more consistent value range from year to year. The adjusted mean NDVI is more stable and got rid of the secondary peak values seen in many annual cycles of the unadjusted mean NDVI curve. The adjusted standard deviation curve is generally above the unadjusted curve and has a reduced range of variation. It is worthwhile to point out that the statistical properties of the ACDF adjusted global NDVI can be expected as a result of the assumptions we made with the ACDF method. Therefore, the more consistent time series of maximum, mean, or standard deviation of the ACDF adjusted NDVI is rather a justification than a validation criterion, particularly considering the known problems and inconsistencies in the unadjusted global NDVI data set over the long term. We will further evaluate the ACDF adjusted NDVI data sets in the following sections.

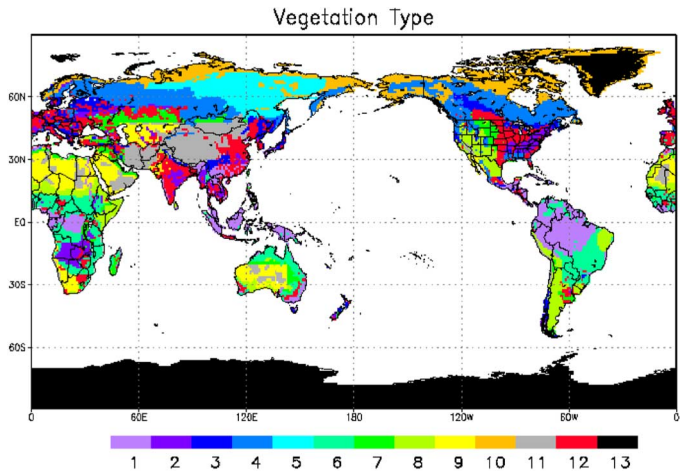

Fig. 4. Thirteen-class global land surface type map: 1) broadleaf-evergreen trees (tropical forest); 2) broadleaf-deciduous trees; 3) broadleaf and needle leaf trees; 4) needle leaf evergreen trees; 5) needle leaf deciduous trees (larch); 6) broadleaf trees with ground cover (savanna); 7) short groundcover (in perennial); 8) broadleaf shrubs with perennial ground cover; 9) broadleaf shrubs with bare soil; 10) tundra (dwarf trees and shrubs with ground cover); 11) bare soil; 12) cropland (cultivated); and 13) glacial.

B. Evaluation for Global Major Land Cover Types

The underlying assumption for the adjustment approaches in this paper is the statistical stationary property of the TOA equivalent NDVI data set at global scale. There is no way to verify the validity of the stationary property of NDVI at global scale without very high quality (e.g., accurate and consistent) global coverage observations. However, it is probably the best assumption to make, considering all sources of errors in the unadjusted NDVI data sets. Although the global-scale trend (e.g., in terms of global mean NDVI) is removed by the stationary assumption of the ACDF approach, the regional trend does not necessarily disappear in the adjusted NDVI data set. Here, we will compare and contrast the unadjusted and the ACDF adjusted NDVI on major land cover types of the globe.

The land type classification map used in the analysis is the 0.144° resolution global land surface vegetation type map which was derived by resampling the 1.0° resolution 13-class vegetation type map in the Global Forecast System [15] currently used at NOAA/NCEP/EMC into a 0.144° resolution latitude/longitude grid (see Fig. 4). These 13 land cover (or vegetation type) classes include: 1) broadleaf-evergreen trees (tropical forest); 2) broadleaf-deciduous trees; 3) broadleaf and needle leaf trees; 4) needle leaf evergreen trees; 5) needle leaf deciduous trees (larch); 6) broadleaf trees with

ground cover (savanna); 7) short groundcover (in perennial); 8) broadleaf shrubs with perennial ground cover; 9) broadleaf shrubs with bare soil; 10) tundra (dwarf trees and shrubs with ground cover); 11) bare soil; 12) cropland (cultivated); and 13) glacial.

Classes 7 and 12 were referred to as grassland and agriculture, respectively, in the Simple Biosphere Model, version 1 (SiB1) vegetation classification [15]. In the derived higher resolution land surface vegetation class map, considering the same or similar parameters used for several classes, the number of classes is regrouped into ten (note: class 13 was excluded from the following analysis) by combining the above classes 7 and 12 into a single class, and classes 8 and 9 into another single class. We chose to combine these classes to increase the sample size in each class.

To further understand the effects after the ACDF adjustment applied to the NDVI data set, we separately evaluated the time series of maximum, mean, and standard deviation of weekly global NDVI for each major land use class (see Fig. 5).

- The maximum values (green lines) for all the classes are more consistent from year to year after the ACDF adjustment than those before the adjustment, although they still have moderate to strong seasonal variations as seen in the unadjusted series.
- The mean values (blue lines) for most classes are larger than the unadjusted series. For class 5—needle leaf deciduous trees, and for class 10—tundra, the two-peak patterns within the annual cycles in the unadjusted series [see the red line in Fig. 5(e)] were reduced to one.
- The ranges of standard deviation values (black lines) are more consistent after the ACDF adjustment.

Note that speaking of peak of maximum values (i.e., not average values), needle leaf deciduous trees' NDVI [Fig. 5(e)] could be as large as that of the tropical forest [Fig. 5(a)]. Part of the reason is that NDVI tends to saturate at very high/dense vegetation value pixels, although in terms of photosynthetic activities, tropical forest is much stronger.

Table II summarizes the 22-year mean and trend (calculated from the least square linear fitting of the annual averaged class mean NDVI series) of the unadjusted and adjusted NDVI for each class, as well as their absolute and relative differences. We can see that the unadjusted NDVI has significant increasing trend over the 22-year period from 1982 to 2003. For example, classes 1, 2, 3, 7 and 12, and 10 have $+15.0\%$, $+15.4\%$, $+18.7\%$, $+17.9\%$, and $+15.3\%$ increase, respectively, for the unadjusted NDVI (see column 4 of Table II); whereas, the adjusted NDVI has much less significant trend (see column 6 of Table II). The overall trend is $+14.9\%$ for the unadjusted global NDVI (excluding class 13—glacial which only accounts for 2% of the total land mass between 75°N and 55°S); whereas, it is only $+0.1\%$ for the adjusted data set. For majority of the classes, the adjusted NDVI are larger than the unadjusted except for classes 4, 5, and 10, while the overall difference is 1.4%. For details, see columns 7 and 8 of Table II.

C. Dependencies on Satellite ECT

There is a dependency of NDVI magnitude on satellite ECT in the unadjusted global NDVI data set, and we expected that this characteristic would be eliminated after the ACDF adjustment. Fig. 6(a) shows the time series of ECT for the operational NOAA polar-orbiting satellites [16] covering the data period in this paper. One of the significant problems in the unadjusted NDVI time series is the obvious dependency on satellite ECTs from different polar orbiters. As an example, Fig. 6(b) depicts the global average NDVI for week 27 (i.e., early July) of different years. The general decreasing trend is obvious for the global mean NDVI from each satellite within its operational period, while the adjusted NDVI gets rid of most of the problem. Note that ECT is not the sole reason for the discrepancies seen in the global mean NDVI time series. Although NOAA-7 and NOAA-9 have very similar ECT shift patterns, there are other major causes that resulted in the fluctuation seen in Fig. 6, which are most likely due to the volcano aerosols emitted by El Chichon from March to April 1982 and Mount Pinatubo in June 1991. For NOAA-16, although ECT shift is not as serious compared to other previous satellites, calibration among still other factors (not yet fully addressed while this paper is being written) probably caused the decreasing trend seen in Fig. 6(b) (from 2002 to 2004).

D. Regional Trend Before and After ACDF Adjustment

To evaluate the regional NDVI after the ACDF adjustment, we analyzed the annual averaged regional NDVI time series for ten major continental-scale regions over the globe. For regions covering high latitudes (e.g., above 60°N) of the Northern Hemisphere, winter weeks were excluded from the analysis because of the spurious signals due to extreme low solar elevation angles and snow cover, and growing season (i.e., from April to October, or weeks 14 to 43) NDVI were averaged for these regions. Fig. 7 presents the annual averaged regional NDVI time series resulted from the unadjusted and adjusted global NDVI data sets for these regions. For regions in Northern Hemisphere mid to high latitudes, we included North America (35°N–75°N, 168°W–55°W, growing season), Europe (35°N–75°N, 11°W–60°E, growing season), Asia (35°N–75°N, 60°E–180°E, growing season), and Contiguous United States (CONUS) (25°N–50°N, 125°W–60°W), as shown in Fig. 7(a)–(d). For regions in Northern Hemisphere low to mid latitudes, we have Africa (0°N–35°N, 18°W–52°E), Asia (0°N–35°N, 55°E–140°E), and Central America (0°N–35°N, 122°W–60°W), as shown in Fig. 7(e)–(g). For regions in Southern Hemisphere, we included South America (0°S–55°S, 83°W–35°W), Africa (0°S–35°S, 18°W–51°E) and Australia (10°S–45°S, 112°E–154°E), and results are shown in Fig. 7(h)–(j). The adjusted NDVIs are larger than the unadjusted ones for these regions and have less interannual variation than the unadjusted series. Much of the increase in the average adjusted NDVI is caused by increases in the anomalously low values for NOAA-7 and NOAA-9 and by the correction in the adjusted data for the effect of much later ECTs as the satellites age. The adjusted global NDVI exhibits more consistent features at the continental scales. Note that it is not directly applicable to draw conclusion on 1988 U.S. drought signal detection using the unadjusted

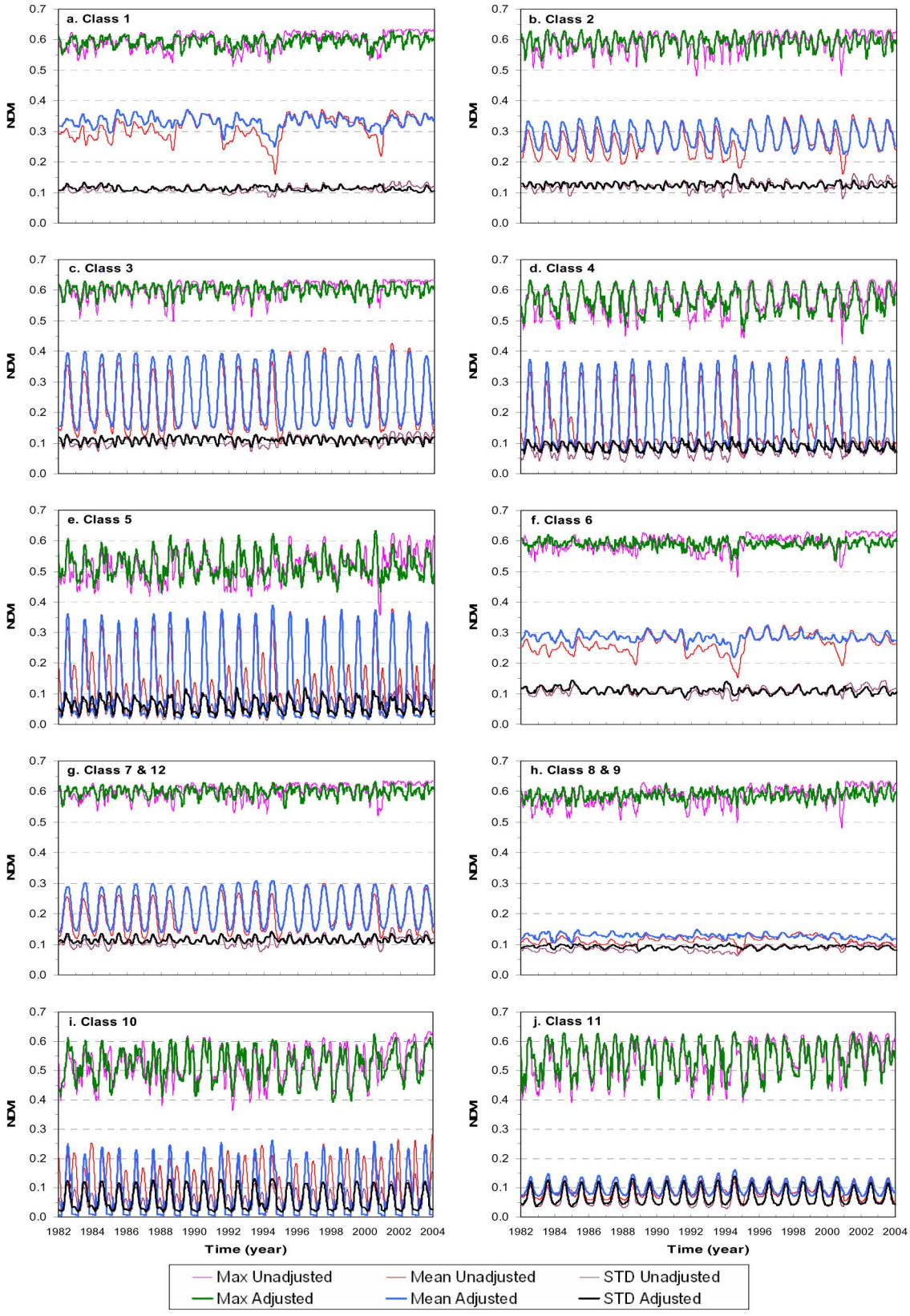

Fig. 5. Unadjusted and adjusted series of maximum, mean, and standard deviation of NDVI within each land surface class from 1982 to 2003.

NDVI, as shown in Fig. 7(d). The annual averaged CONUS domain mean NDVI is not sufficient for one to infer drought for a particular week, month, or season. Moreover, the low annual CONUS mean NDVI for 1988, as seen in Fig. 7(d), is more likely due to the NOAA-9 AVHRR sensor's serious degradation, which is evident in Fig. 6, and caused the obvious

TABLE II
COMPARISON OF UNADJUSTED AND ACDF-ADJUSTED NDVI FOR DIFFERENT LAND CLASSES

Class	Pixels%	Unadjusted		Adjusted		Absolute difference	Relative Difference
		Mean of Annual Averaged NDVI	Trend from 1982 to 2003	Mean of Annual Averaged NDVI	Trend from 1982 to 2003		
1	8.95%	0.312	+15.0%	0.332	-0.6%	0.020	6.4%
2	4.01%	0.262	+15.5%	0.282	-0.0%	0.020	7.6%
3	4.35%	0.237	+18.7%	0.255	+3.4%	0.017	7.2%
4	13.68%	0.185	+13.1%	0.184	+1.9%	-0.001	-0.8%
5	7.11%	0.161	+4.4%	0.133	-4.2%	-0.028	-17.4%
6	9.67%	0.263	+13.2%	0.285	-1.2%	0.022	8.4%
7 & 12	16.57%	0.199	+17.9%	0.217	+2.3%	0.018	9.1%
8 & 9	15.22%	0.113	+2.9%	0.128	-4.4%	0.015	13.0%
10	9.86%	0.129	+15.3%	0.080	+4.9%	-0.049	-37.9%
11	8.79%	0.088	+3.5%	0.100	-2.8%	0.011	12.8%
Overall	98.00%	0.186	+14.9%	0.189	+0.1%	0.003	1.4%

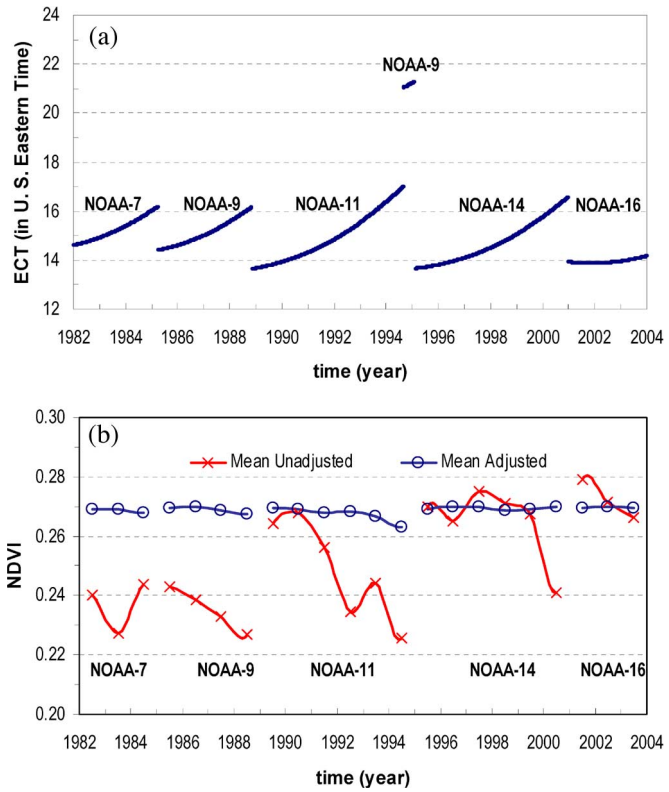

Fig. 6. (a) Satellite ECTs for the period 1982 to 2003. (b) Global mean of unadjusted and adjusted NDVI for week 27 from 1982 to 2993.

lower-than-normal global mean NDVI values seen in Fig. 1 (thick black line).

Table III compares the unadjusted and adjusted global NDVI in terms of mean of the annual averaged NDVI and 22-year trend in the annual averaged NDVI series (calculated from the linear fitting of the annual averaged regional NDVI series), as well as their differences for the above ten regions. For the unadjusted regional NDVI, the 22-year trends are all positive for these regions, and the trends are very large (e.g., more than 15%) for regions such as Europe (+27.6%), North America (+19.4%), Asia (low to mid latitude, +17.7%), Asia (mid to high latitude, +15.9%), CONUS (+15.6%), and Central America (+15.4%); whereas the adjusted NDVI have much smaller to even negative trends for these regions, e.g., +8.5% for Europe, +1.4% for North America, and −0.0% for Asia (low to mid latitude). For other details, see Table III. Together with Fig. 7, these results imply that after the global-scale ACDF adjustment to NDVI, the very large regional-scale NDVI satellite-to-satellite variations in the unadjusted NDVI data sets are suppressed, and the very large regional vegetation increasing trend for the 22-year period are significantly reduced. However, although the variations caused by instrument change and equator-crossing drift are suppressed, local vegetation anomalies due to drought and abnormally favorable weather are retained in the data.

E. Evaluation by Applications on Regional Severe Droughts

Regional droughts (resulting from long lasting below normal precipitation amount and/or high temperature) can cause below normal vegetation growth and maturation. Presently, one of the important applications of global NDVI (resulting from the NOAA GVI2 data sets) is the detection of regional drought. However, as can be inferred from Fig. 7 and Table III, with a large satellite-caused trend of regional NDVI in the unadjusted global NDVI data sets, drought detection becomes harder. In a particular region, the indicator of drought for a certain period of a year may be marked by the abnormally low NDVI compared to a multiyear average or by the extent to which the real-time NDVI approaches the known historical minimum NDVI. The latter forms the basis of the vegetation condition index (VCI) defined as

$$\mathrm{VCI} = \frac{\mathrm{ND} - \mathrm{ND}_{\min}}{\mathrm{ND}_{\max} - \mathrm{ND}_{\min}} \cdot 100 \tag{4}$$

where $\mathrm{ND}_{\min}$ and $\mathrm{ND}_{\max}$ are the climatological minimum and maximum NDVI, respectively, within the known data sets. Note that these quantities are rederived after the ACDF adjustment, thus $\mathrm{ND}_{\min}$ and $\mathrm{ND}_{\max}$ in the adjusted data set are different from those in the unadjusted data set. ND is the real-time NDVI. We refer to [4], [17], and [18] for detailed discussions on VCI and its applications. VCI normally ranges

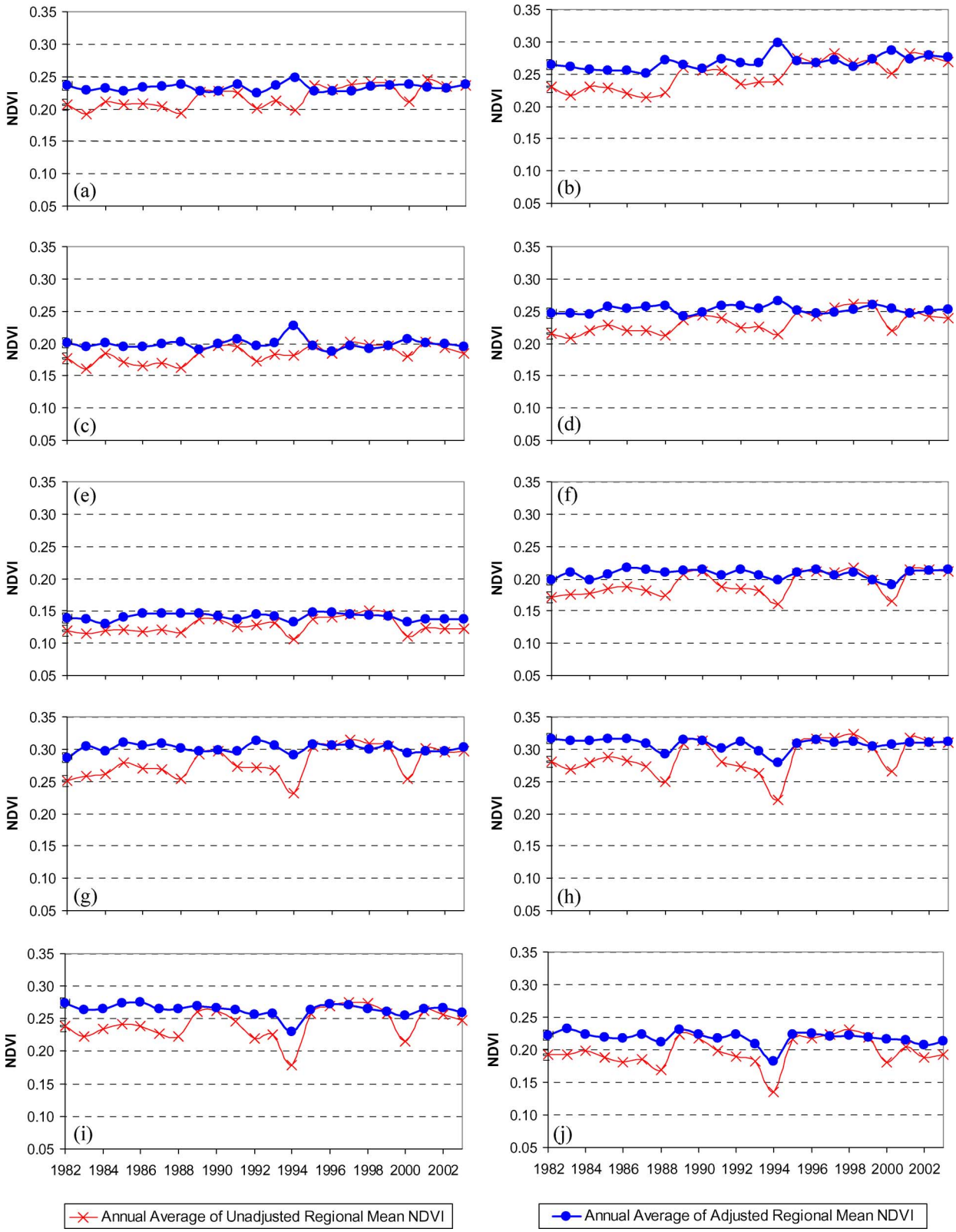

Fig. 7. Annual averaged series of unadjusted and adjusted spatial mean NDVI for ten regions of the globe. (a) North America Growing Season [35N–75N, 168W–55W]. (b) Europe Growing Season [35N–75N, 11W–60E]. (c) Asia (Mid to High Latitude) Growing Season [35N–75N–60E–180E]. (d) CONUS U.S. [25N–50N, 125W–60W]. (e) Africa (Northern Hemisphere) [0N–35N, 18W–52E]. (f) Asia (Low to Mid Latitude) [0N–35N, 55E–140E]. (g) Central America [0N–35N, 120W–60W]. (h) South America [0S–55S, 83W–35W].

between 0 and 100. Low VCI values (e.g., below 40) indicate abnormally low vegetation growth, whereas high VCI values (e.g., above 60) indicate the opposite.

Here, we separately apply (4) to the unadjusted and ACDF adjusted NDVI data sets and show the application of VCI to the detection of 2005 U.S. droughts. As reported from ground

TABLE III
COMPARISON OF SPATIALLY AVERAGED UNADJUSTED AND ACDF ADJUSTED NDVI FOR DIFFERENT REGIONS FROM 1982 to 2003

	Region	Unadjusted		Adjusted		Absolute difference	Relative Difference
		Mean of Annual Averaged NDVI	Trend from 1982 to 2003	Mean of Annual Averaged NDVI	Trend from 1982 to 2003		
Northern Hemisphere (mid to high latitude)	**North America** (35N~75N, 168W~55W) growing season	0.219	+19.4%	0.233	+1.4%	0.014	6.4%
	Europe (35N~75N, 11W~60E) growing season	0.249	+27.6%	0.268	+8.5%	0.019	7.6%
	Asia (35N~75N, 60E~180E) growing season	0.184	+15.9%	0.199	+0.2%	0.015	8.3%
	CONUS U. S. (25N~50N, 125W~60W) all year	0.233	+15.6%	0.252	+0.5%	0.020	8.4%
Northern Hemisphere, (low to	**Africa** (0N~35N, 18W~52E) all year	0.127	+9.7%	0.141	-0.9%	0.014	11.0%
	Asia (0N~35N, 55E~140E) all year	0.192	+17.7%	0.207	-0.0%	0.015	7.8%
	Central America (0N~35N, 122W~60W) all year	0.280	+15.4%	0.301	-0.0%	0.021	7.6%
Southern Hemisphere	**South America** (0S~55E, 83W~35W) all year	0.289	+13.1%	0.308	-1.6%	0.020	6.8%
	Africa (0S~35S, 18W~51E) all year	0.243	+10.2%	0.264	-3.6%	0.021	8.8%
	Australia (10S~45S, 112E~154E) all year	0.197	+7.2%	0.218	-5.1%	0.021	10.8%

observations and demonstrated by the U.S. Drought Monitor (online at http://www.drought.unl.edu/dm/monitor.html), there are moderate to severe droughts from the northeast to central U.S. in the growing season of 2005.

Fig. 8 presents the VCI from the unadjusted and ACDF-adjusted NDVI for weeks 20 (May), 29 (July), and 37 (September) of 2005. We can see that the VCI from the ACDF-adjusted NDVI demonstrate much stronger drought signals (i.e., low VCI value clusters) than those from the unadjusted NDVI. It is this feature of the ACDF-adjusted NDVI that makes it useful for drought detection and as a source of GVF for NWP boundary conditions.

To further demonstrate the impact on regional severe drought detection using the ACDF-adjusted NDVI data set as oppose to the unadjusted NDVI, we have selected 14 cases of severe regional droughts and compared regional averaged standardized NDVI anomalies from the unadjusted and ACDF-adjusted NDVI data sets. The standardized NDVI anomaly is defined as

$$\mathrm{ND}^* = \frac{\mathrm{ND} - \overline{\mathrm{ND}}}{\sigma_{\mathrm{ND}}} \tag{5}$$

where ND^* is the standardized NDVI, and $\overline{\mathrm{ND}}$ and σ_{ND} are the average and the standard deviation of NDVI, respectively, in the time series of our sample data set from 1982 to 2003. More negative ND^* value indicates stronger below normal growth for vegetation, which is often the consequence of severe drought.

Table IV shows the comparisons of regional mean ND^* for 14 drought cases. These droughts occurred at four major continents over 14 years (e.g., from 1985 to 1998), covering various climatic regions. Column 2 of this table indicated the region, spatial range, and time (e.g., week number and year number) for these drought occurrences. Detailed descriptions of these droughts can be found in [4] (for cases i and j), [5] (for cases b, c, d, k, l, m, and n), [6] (for cases e, f, g, and h), and [17] (for cases a, b, and c). These droughts were severe enough that, in the past, even the unadjusted NDVI can detect the strong anomaly signals, as shown in column 3 of Table IV. Column 4 of Table IV shows that, except for case b, the ACDF-adjusted NDVI had a similar or enhanced level of negative vegetation anomaly signals, compared to column 3. Although it is a limited number of cases, our results provided evidence that the global stationarity assumption in the ACDF approach does not imply regional stationarity.

IV. DISCUSSION

There are limitations within the present study scope. The first is related to the lack of comprehensive validation for the historical global NDVI data sets because direct ground-based

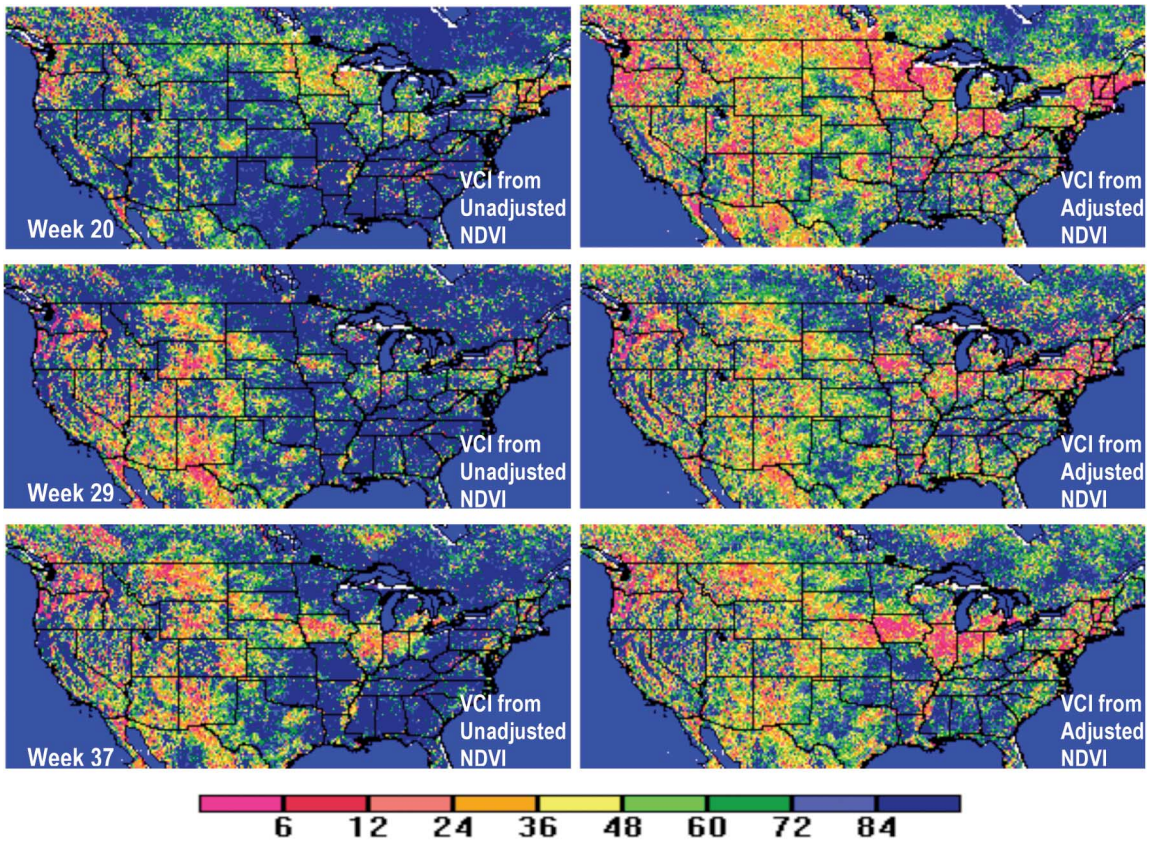

Fig. 8. Comparison of VCI resulting from unadjusted and adjusted NDVI data sets over the CONUS U.S. (27°N–53°N, 127°W–67°W) in 2005 for weeks 20 (May), 29 (July), and 37 (September).

TABLE IV
COMPARISON OF REGIONAL NDVI ANOMALIES FROM THE UNADJUSTED AND THE ADJUSTED GLOBAL NDVI DATA SETS

Continent	Region, Spatial Range and Time	Standardized Anomaly from Un-adjusted NDVI	Standardized Anomaly from ACDF adjusted NDVI
North America	a. Great Plains, USA, (40~50N, 102~110W), wk 26, 1985	-1.79	-1.72
	b. Great Plains, USA, (35~43N, 85~100W), wk 26, 1988	-2.41	-1.44
	c. Great Plains, USA, (35~42N, 95~104W), wk 19, 1989	-1.58	-1.72
	d. Great Plains, USA, (30~40N, 95~102W), wk 13, 1996	-1.71	-2.08
South America	e. Argentina, (28~35S, 60~68W), wk 51, 1988	-2.33	-2.15
	f. Argentina, (30~45S, 64~70W), wk 51, 1989	-1.18	-1.82
	g. Argentina, (38~42S, 64~68W), wk 50, 1995	-0.59	-0.67
	h. Argentina, (31~45S, 63~68W), wk 4, 1996	-1.32	-1.61
Africa	i. Zimbabwe, (19 ~ 23S, 28 ~ 33E), wk 51, 1991	-1.23	-1.20
Euro– Asia	j. FSU, (40~55N, 45~60E), wk 31, 1986	-1.50	-1.27
	k. FSU, (48~55N, 59~75E), wk 24, 1991	-1.28	-1.67
	l. FSU, (44~50N, 62~73E), wk 26, 1995	-1.14	-1.26
	m. FSU, (43~48N, 53~68E), wk 26, 1996	-1.35	-1.38
	n. FSU, (50~54N, 58~68E), wk 26,1998	-1.11	-1.76

or other independent observations are not available, except for a few limited regions. It is doubtful that the ground data from a few local field campaigns are of much use to validate a global data set, although they can provide useful insights on sensor performance for specific areas under specific environmental conditions.

The second limitation is the lack of full physics-based corrections to the raw remote sensing data from which NDVI

was derived. The weekly global SMN based on the operational AVHRR data, although derived after the best known prelaunch and postlaunch calibrations, lack operational globally consistent correction procedures for atmospheric effects, sun–earth–target geometry variation, and spectral variation from one sensor to the next. Even after the recent effort by NOAA/NESDIS scientists to reprocess the AVHRR global area coverage data and thereby establish a global vegetation CDR, the temporal discrepancies in NDVI arising from different generations of sensors remain an issue.

The third limitation is the assumption of the stationary property on the interannual total global vegetation amount for a week. If the Earth is greening, as several studies based on the AVHRR record have suggested, then our assumption of stationarity is incorrect. However, the long-term studies of "global greening" must deal with the problems of calibration, orbit drift, and spectral changes from AVHRR/1 through AVHRR/3. None, so far, have dealt with all of these issues, so the magnitude of long-term greening, which is inferred from the AVHRR data set, is still an open question. Another shortcoming related to this assumption is that smooth variation cannot, in a strict sense, be used as a criterion for validation. In the context of this paper, we use the smooth and consistent variation of global NDVI as a justification for a quality-improved global data set over the long term, considering the known problems and inconsistencies in the unadjusted global NDVI data set.

For purposes of initialization of weather forecast models with AVHRR GVF, the ACDF-adjusted NDVI is superior to the uncorrected data. The errors in GVF eliminated by the ACDF procedure are significant and known. If the lack of global stationarity becomes a problem as the greenness of the Earth changes over the long term, then the climate reference data set years (1989, 1990, 1995, 1996, 1997, and 1998) will have to be changed to accommodate the changing greenness of the Earth in later years.

V. Conclusion

A number of different simple one-step (e.g., RRS, RRS_Top 1%, NML, LR, and ACDF) global adjustment approaches have been investigated in this paper. Combined uses of such procedures (e.g., NML_RRS and SBS_NML) are also investigated, and results are briefly described together with the one-step approaches.

Most of these approaches need a benchmark annual cycle from the 52-week global NDVI climatology, which uses the best quality and most temporally stable NDVI data available from 6 of the 22 years (1989, 1990, 1995, 1996, 1997, and 1998, composed of NOAA-11 and -14 data). Overall, among the approaches investigated here, we conclude that the ACDF approach produces a temporally more consistent historical data set of global NDVI over the past two decades, reasonably free of false temporal trends from sensor aging or change in sensor spectral bandwidth or equatorial crossing time. Given its simplicity, it can be implemented in near real-time weekly operations of NESDIS AVHRR-based NDVI data processing with minimum overhead. Our future effort will be to derive the GVF, which is used by the operational weather and climate models at NOAA/NCEP/EMC from the ACDF-adjusted NDVI data set in an operational manner.

Acknowledgment

The authors would like to thank Dr. A. Ignatov of NOAA/NESDIS/STAR for the information regarding NOAA polar-orbiting satellite ECT and Dr. J. T. Sullivan of NOAA/NESDIS/STAR for the comments during various stages of this study. The contents of this paper are solely the opinions of the authors and do not constitute a statement of policy, decisions, or position on behalf of NOAA or the U.S. Government.

References

[1] K. B. Kidwell, *Global Vegetation Index User Guide. U.S. Dept. of Commerce, NOAA/NESDIS*. Asheville, NC: Satellite Data Services Division, Nat. Climatic Data Center, 1994.

[2] G. Gutman, D. Tarpley, A. Ignatov, and S. Olson, "The enhanced NOAA global land data set from the Advanced Very High Resolution Radiometer," *Bull. Amer. Meteorol. Soc.*, vol. 76, no. 7, pp. 1141–1156, Jul. 1995.

[3] F. N. Kogan, "Remote sensing of weather impacts on vegetation in nonhomogeneous areas," *Int. J. Remote Sens.*, vol. 11, pp. 1405–1419, 1990.

[4] F. N. Kogan, "Global drought watch from space," *Bull. Amer. Meteorol. Soc.*, vol. 78, no. 4, pp. 621–636, Apr. 1997.

[5] F. N. Kogan, "Operational space technology for global vegetation assessment," *Bull. Amer. Meteorol. Soc.*, vol. 82, no. 9, pp. 1949–1964, Sep. 2001.

[6] R. A. Seiler, F. Kogan, and W. Guo, "Monitoring weather impact and crop yield from NOAA AVHRR data in Argentina," *Adv. Space Res.*, vol. 26, no. 7, pp. 1177–1185, 2000.

[7] J. D. Tarpley, S. R. Schneider, and R. L. Money, "Global vegetation indices from the NOAA-7 meteorological satellite," *J. Clim. Appl. Meteorol.*, vol. 23, no. 3, pp. 491–494, Mar. 1984.

[8] R. B. Myneni, C. D. Keelivolng, C. J. Tucker, G. Asrar, and R. R. Nemani, "Increased plant growth in the northern high latitudes from 1981 to 1991," *Nature*, vol. 386, no. 6626, pp. 698–702, Apr. 1997.

[9] L. L. Stowe, R. M. Carey, and P. P. Pellegrino, "Monitoring the Mt. Pinatubo aerosol layer with NOAA/11 AVHRR data," *Geophy. Res. Lett.*, vol. 19, no. 2, pp. 159–162, Jan. 1992.

[10] G. Gutman and A. Ignatov, "The derivation of the green vegetation fraction from NOAA/AVHRR data for use in numerical weather prediction models," *Int. J. Remote Sens.*, vol. 19, no. 8, pp. 1533–1543, May 1998.

[11] M. B. Ek, K. E. Mitchell, Y. Lin, E. Rogers, P. Grunmann, V. Koren, G. Gayno, and J. D. Tarpley, "Implementation of NOAA land surface model advances in the National Centers for Environmental Prediction operational mesoscale Eta model," *J. Geophys. Res.*, vol. 108, no. D22, 8851, 2003. DOI: 10.1029/2002JD003296.

[12] C. R. N. Rao and J. Chen, "Inter-satellite calibration linkages for the visible and near-infrared channels of the advanced very high resolution radiometer on the NOAA-7, -9, and -11 spacecraft," *Int. J. Remote Sens.*, vol. 16, pp. 1931–1942, 1995.

[13] X. Wu, "Operational calibration of AVHRR/3 solar reflectance channels," in *Proc. Conf. Characterization Radiometric Calibration for Remote Sens.* Logan, UT: Utah State Univ., Aug. 2004.

[14] A. van Dijk, S. L. Callis, C. M. Sakamoto, and W. L. Decker, "Smoothing vegetation index profiles: An alternative method for reducing radiometric disturbance in NOAA/AVHRR data," *Photogramm. Eng. Remote Sens.*, vol. 53, pp. 1059–1067, 1987.

[15] P. J. Sellers, S. O. Los, C. J. Tucker, C. O. Justice, D. A. Dazlich, G. J. Collatz, and D. A. Randall, "A revised land surface parameterization (SiB2) for atmospheric GCMs—Part II: The generation of global fields of terrestrial biophysical parameters from satellite data," *J. Clim.*, vol. 9, no. 4, pp. 706–736, Apr. 1996.

[16] A. Ignatov, I. Laszlo, E. D. Harrod, K. B. Kidwell, and G. P. Goodrum, "Equator crossing times for NOAA, ERS and EOS sun-synchronous satellites," *Int. J. Remote Sens.*, vol. 25, no. 23, pp. 5255–5266, Dec. 2004.

[17] F. N. Kogan, "Droughts of the late 1980s in the United States as derived from NOAA polar orbiting satellite data," *Bull. Amer. Meteorol. Soc.*, vol. 76, no. 5, pp. 655–668, May 1995.

[18] F. N. Kogan and X. Zhu, "Evolution of long-term errors in NDVI time series: 1985–1999," *Adv. Space Res.*, vol. 28, no. 1, pp. 149–153, 2001.

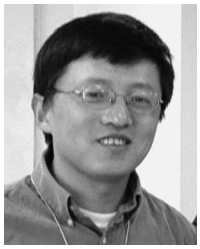

Le Jiang received the B.Sc. degree in atmospheric science from Nanjing University, Nanjing, China, in 1991 and the Ph.D. degree in earth system science from the University of Cincinnati, Cincinnati, OH, in 2000.

He is with I. M. Systems Group, Inc. (IMSG), National Oceanic and Atmospheric Administration (NOAA), National Environmental Satellite, Data, and Information Service (NESDIS), Camp Springs, MD, where he is the Chief Scientist/Program Manager. He is currently leading the IMSG scientific and technical support teams at NOAA/NCEP/EMC and NOAA/NESDIS/STAR on algorithm development, satellite applications, and research. He had developed the satellite-based methodology for land surface evapotranspiration monitoring and improved the operational algorithms for AVHRR-based global vegetation monitoring, among others. He is an Affiliate Member of the IEEE Geoscience and Remote Sensing Society.

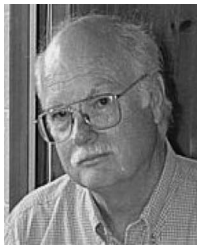

J. Dan Tarpley is with the Center for Satellite Applications and Research, National Oceanic and Atmospheric Administration, National Environmental Satellite, Data, and Information Service (NESDIS), Camp Springs, MD, as the Chief of the Environmental Monitoring Branch, Satellite Meteorology and Climatology Division, where he leads the land remote sensing activities. His interests include development and use of remotely sensed snow cover, vegetation conditions, surface albedo, surface radiation budget, and precipitation products for validation and boundary conditions in NWP models.

Kenneth E. Mitchell received the B.Sc., M.Sc., and Ph.D. degrees in meteorology from The Pennsylvania State University, University Park, in 1973, 1975, and 1979, respectively.

He worked in numerical weather prediction model development at the Air Force Global Weather Center from 1978 to 1982 and at the Air Force Geophysics Laboratory from 1982 to 1988. Since 1989, he has been with the Environmental Modeling Center, National Oceanic and Atmospheric Administration, National Centers for Environmental Prediction (NCEP), Camp Springs, MD, where he focuses on land surface modeling in NCEP weather and climate prediction models spanning short-range regional mesoscale models to seasonal-range global models.

Sisong Zhou received the B.Sc. degree in meteorology from the Nanjing University of Information Science and Technology, Nanjing, China.

He was a scientist in the field of satellite remote sensing. In 2006, he retired from I. M. Systems Group, Inc., National Oceanic and Atmospheric Administration (NOAA), National Environmental Satellite, Data, and Information Service (NESDIS), Camp Springs, MD. From 1991 to 2006, he was a Support Scientist at NOAA/NWS and NOAA/NESDIS. From 1989 to 1991, he was a Senior Resident Research Associate at the National Research Council (USA). From 1971 to 1989, he was with the National Satellite Meteorological Center of China.

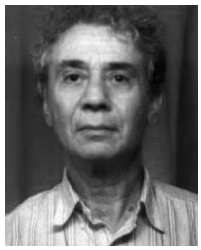

Felix N. Kogan received the Ph.D. degree in environmental sciences from the World Meteorological Center (WMC), Moscow, Russia.

He was with the Institute for Agricultural Meteorology, Obnisk, Russia, the WMC, Moscow, and the University of Missouri, Columbia. He is currently with the Center for Satellite Application and Research, National Oceanic and Atmospheric Administration, National Environmental Satellite, Data, and Information Service (NESDIS), Camp Springs, MD. His works include research and development in the application of satellite data to land and atmosphere, development of long-term AVHRR data sets, assessment of the impact of climate and weather on human activities, climate variability, and environmental hazards.

Wei Guo received the M.S. degree in satellite meteorology from Peking University, Beijing, China, in 1990.

He has been a Senior Scientific/System Programmer with I. M. Systems Group, Inc., National Oceanic and Atmospheric Administration (NOAA), National Environmental Satellite, Data, and Information Service (NESDIS), Camp Springs, MD since 2002. He was with the National Satellite Meteorology Center of China, University of Virginia, Charlottesville, University of Maryland, College Park, and Center for Satellite Application and Research, NOAA/NESDIS, Camp Springs. His works include scientific data analysis, application software, and utility tool development to support land surface remote sensing R&D.